Superconductor Science and Technology

Asymmetric behaviour of $J_c(\varepsilon)$ in Nb_3Sn wires and correlation with the stress induced elastic tetragonal distortion

To cite this article: R Flükiger *et al* 2005 *Supercond. Sci. Technol.* **18** S416

View the article online for updates and enhancements.

You may also like

- Mechanical and superconducting properties of Nb_3Sn wires with Nb-rod-processed CuNb reinforcement
Hidetoshi Oguro, Satoshi Awaji, Kazuo Watanabe et al.
- Effect of Zn addition and Ti doping position on the diffusion reaction of internal tin Nb_3Sn conductors
Nobuya Banno, Taro Morita, Zhou Yu et al.
- The effects of Mg doping on the microstructure and transport properties of internal tin-processed brass matrix Nb_3Sn superconductors
Zhou Yu, Nobuya Banno, Yong Zhao et al.

This content was downloaded from IP address 18.116.36.192 on 23/04/2024 at 08:28

INSTITUTE OF PHYSICS PUBLISHING SUPERCONDUCTOR SCIENCE AND TECHNOLOGY

Supercond. Sci. Technol. **18** (2005) S416–S423 doi:10.1088/0953-2048/18/12/032

Asymmetric behaviour of $J_c(\varepsilon)$ in Nb_3Sn wires and correlation with the stress induced elastic tetragonal distortion

R Flükiger, D Uglietti, V Abächerli and B Seeber

Group of Applied Physics (GAP) and Department of Physics of Condensed Matter (DPMC), University of Geneva, 1211 Geneva, Switzerland

Received 6 September 2005, in final form 6 October 2005
Published 16 November 2005
Online at stacks.iop.org/SUST/18/S416

Abstract

The effect of uniaxial strain on the critical current of 0.8 m long Nb_3Sn wires up to 21 T is studied by the modified Walters spring (WASP). For Nb_3Sn wires, prepared by both the bronze route and the internal Sn diffusion process, the critical current density as a function of the uniaxial strain ε is found to exhibit an asymmetric behaviour on both sides of the strain ε_m, where J_c reaches its maximum. Revisiting earlier x-ray and neutron diffraction measurements on bronze route processed wires between 10 and 600 K, it is shown that the asymmetric behaviour of $J_c(\varepsilon)$ on both sides of the strain value ε_m is connected to individual variations of the stress-induced tetragonal lattice parameters a and c.

The present measurements of J_c versus strain for Nb_3Sn wires show stronger strain dependence for wires prepared by the internal Sn diffusion method with respect to those obtained by the bronze route. The reasons for this difference are attributed to the individual details of the filament configuration in both types of wire, for example the different Sn distributions inside the filaments and the very different filament sizes, 4 and 80 μm, respectively.

(Some figures in this article are in colour only in the electronic version)

1. Introduction

A characteristic property of multifilamentary Nb_3Sn wires in high magnetic fields is the sensitivity of the critical current density, J_c, to the mechanical loads caused by the Lorentz forces. The resulting forces can be tensile and/or compressive, the ratio between them depending on the operation field and on the size of the applied device of interest. In small-bore magnets, e.g. NMR solenoids, the main stress component at magnetic fields as high as 21 T will be tensile. In large devices, e.g. Tokamak magnets (∼12 T) or future dipoles for accelerators (∼15 T), both tensile and compressive forces are acting on the conductors. The precise knowledge of J_c for a given conductor under operational stress/strain conditions, i.e. as a function of B, T and ε, is of fundamental importance for optimizing both performance and costs, regardless of the nature of the device.

For both wire types, an asymmetric behaviour of $J_c(\varepsilon)$ is observed at all fields on both sides of ε_m. An explanation of this asymmetry is given, based on previous x-ray and neutron diffraction measurements, which show a variation of the lattice parameters a and c of the elastically distorted tetragonal Nb_3Sn phase as a function of both T and ε.

In the present paper, we compare the stress sensitivity of two Nb_3Sn wires, produced by the bronze route process and the internal Sn diffusion technique, respectively. The modified Walters spiral and the $I_c(\varepsilon)$ results up to 21 T are presented, showing a stronger strain sensitivity for internal Sn diffusion wires. This difference between the two wire types is briefly discussed on the basis of the individual wire configurations.

2. The modified Walters spiral (WASP)

Compared to other devices for the measurement of $I_c(\varepsilon)$ [1, 2], the Walters spiral [3, 4] allows one to measure considerably longer samples. A modified version of the Walters spiral (WASP) has been constructed in Geneva for measurements up to currents of 1000 A and fields up to 21 T [5, 6]. A

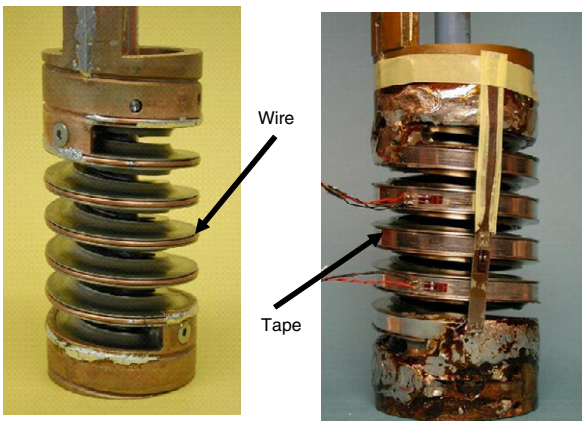

Figure 1. Different types of modified Walters spring (WASP), for round/rectangular wires and for tapes.

Table 1. Wire design parameters.

Wire	Composition	Diameter (mm)	Filaments	Fil. size (μm)	Cu/ non-Cu
GAP, #24	(Nb, Ta, Ti)$_3$Sn	1.25	14 641	4	0.25
OST, #7069	(Nb, Ti)$_3$Sn	0.8	18[a]	80[b]	1.5

[a] Agglomerated filament bundles.
[b] Effective diameter of a bundle.

more detailed description of this device has recently been published [7]. The wire samples are mounted onto the WASP and can be strained either under compression or under tension by keeping one end of the spring in position and by rotating the other one. The spring consists of Ti6Al4V, thus allowing the application of reversible and linear strains ε above 1% at 4.2 K. The total wire length is 0.8 m, and the voltage tap distance can reach up to 0.60 m, which has two positive consequences: (a) there is no current transfer problem and (b) a voltage criterion as stringent as 0.01 μV cm^{-1} can be applied. This constitutes a progress in view of the precise characterization of superconducting wires. Several spiral modifications with different groove sizes have been built (figure 1), in order that both rectangular and round wires with various cross sections as well as YBCO-coated conductor tapes can be measured. The top of the WASP can be rotated by a dc motor located outside of the cryostat, a piezoelectric sensor measuring the torque, while the angular position of the motor can be determined by an opto-encoder. The value of the strain ε is determined with a high precision [5–7]: a first measurement is performed in the stress-free state, $\varepsilon = 0$, at the original value of J_c, and this serves as a calibration point for the second measurement with the wire soldered on the WASP. The present device allows one to exert an additional precompression on the wire, corresponding to an intrinsic strain $\varepsilon_{intrinsic} = \varepsilon_m - \varepsilon$ up to -1% (ε_m is the strain at which J_c reaches its maximum).

3. The wire configurations

The design parameters of the bronze route and of the internal Sn diffusion wires used in the present are summarized in table 1.

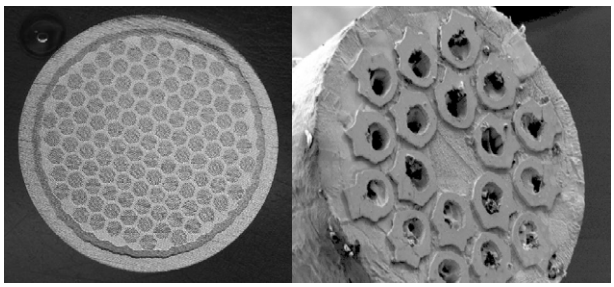

Figure 2. Cross sections of Nb_3Sn wires. Left: bronze route processed; right: internal Sn diffusion processed (after reaction, showing large, agglomerated filaments).

3.1. The bronze route wire (GAP)

The Nb_3Sn wire #24 produced in our laboratories at GAP [8] was manufactured using Nb–7.5 wt% Ta rods for the filaments and an Osprey-processed Cu–Sn bronze with 15.6 wt% Sn, doped with 0.25% Ti. The deformation process to obtain wires with a final diameter of about 1 mm requires three hot hydrostatic extrusion steps. Before the third extrusion, an external Nb barrier and a copper stabilization are added. After the third extrusion step, the rods consisting of 14 641 filaments were drawn into round conductors of 1.25 mm diameter and $\sim$100 m length. The local bronze/filament ratio (for the filament bundles after the second extrusion step) was chosen to be 2.2, while the global ratio was 2.5. The reaction conditions were 600 °C/100 h–670 °C/150 h, the heating and cooling rates being 30 °C h^{-1} [8].

3.2. The internal Sn diffusion wire (OST)

The internal Sn diffusion processed wire (RRP type, #7069) with the composition (Nb, Ti)$_3$Sn was manufactured by Oxford Superconducting Technology (OST) [9]. It is a round wire (0.8 mm diameter), consisting of 18 cylindrical bundles, each one consisting of several hundreds of agglomerated filaments. Filaments are made of Nb tubes inserted in a copper matrix, Sn being introduced inside the Nb tubes. The wire #7069 had a non-Cu critical current density of about 2500 A mm^{-2} at 12 T and 4.2 K.

The filaments in the bronze route wire have a size around 4 μm, while the internal Sn diffusion wire undergoes an agglomeration process, which results in an effective filament diameter of the order of 80 μm. Cross sections of both wires are represented in figure 2.

4. Comparison between the behaviour of $J_c(\varepsilon)$ for both wire types

The GAP and OST wires are characterized in table 2 for fields of 17 and 21 T. The internal Sn wire contains a higher amount of Nb_3Sn with respect to bronze route wires, the ratio between the values of $J_{c(Non-Cu)}$ for the OST and the GAP wires at 21 T and $\varepsilon = \varepsilon_m$ being 2.84. However, internal Sn diffusion wires require a considerably higher amount of stabilizing Cu, in order that this ratio decreased to 1.42 for the $J_{c(overall)}$ values at same field. The critical current density of both wire types as a function of the applied field B is represented in figure 3,

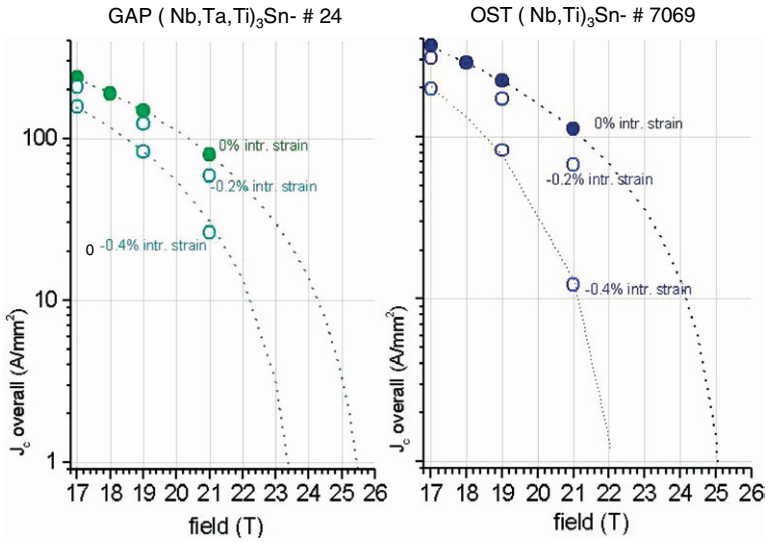

Figure 3. J_c versus B at 4.2 K for the Nb_3Sn wires produced by the bronze route process (left) and by the internal Sn diffusion technique (right). The curves are fitted according to [1], under the intrinsic strains −0.4, −0.2 and 0%.

Table 2. Critical current densities for 0% intrinsic strain, at 4.2 K. Criterion: 0.1 μV cm^{-1}.

Wire	ε_m (%)	$J_{c\ non-Cu}$ at 17 T (A mm^{-2})	$J_{c\ overall}$ at 17 T (A mm^{-2})	$J_{c\ non-Cu}$ at 21 T (A mm^{-2})	$J_{c\ overall}$ at 21 T (A mm^{-2})
GAP, #24	0.25	294	235.5	99	79.5
OST, #7069	0.25	910	364	281	112.5

for the strain values $\varepsilon_{intrinsic} = \varepsilon_m - \varepsilon = -0.4$, -0.2 and 0%, respectively. In both cases, the strain ε_m was found to be 0.25% (table 2). The strain value $\varepsilon_{intrinsic} = -0.4\%$, representing an additional precompression (compared to the as-reacted state), was obtained by inverting the rotation direction of the WASP. Figure 4 shows the normalized values $I_c(\varepsilon)/I_{c0}$ of the bronze route (GAP) wire, at 17, 19 and 21 T, respectively, while the corresponding results for the internal Sn diffusion wire are shown in figure 5. A comparison of the normalized critical densities $I_c(\varepsilon)/I_{c0}$ between the two wire types at 21 T is shown in figure 6. It appears that $I_c(\varepsilon)/I_{c0}$ of the internal Sn diffusion wire shows a considerably stronger variation than that of the bronze route wire. In figure 7, it is shown that the exponential $n(\varepsilon)$ value also reaches a maximum at ε_m, the values being similar for both wires.

The question of the higher strain sensitivity for the internal Sn diffusion wire is of particular interest. In the internal Sn diffusion wire (OST), the A15 phase contains a ternary addition, Ti, while the bronze route (GAP) wire contains two additives, Ta and Ti. It was published earlier [10–13] that the ratio $I_c(\varepsilon)/I_{c0}$ of alloyed Nb_3Sn wires is less strain sensitive than that for binary ones, the effect of alloying being a shortening of the electronic mean free path, which in turn leads to higher B_{c2} values. Since both wires studied in the present work are alloyed, one expects similar values for B_{c2}. Taking the data of figure 3, a rough extrapolation indeed yields B_{c2} values between 25 and 26 T for both wires, the uncertainty

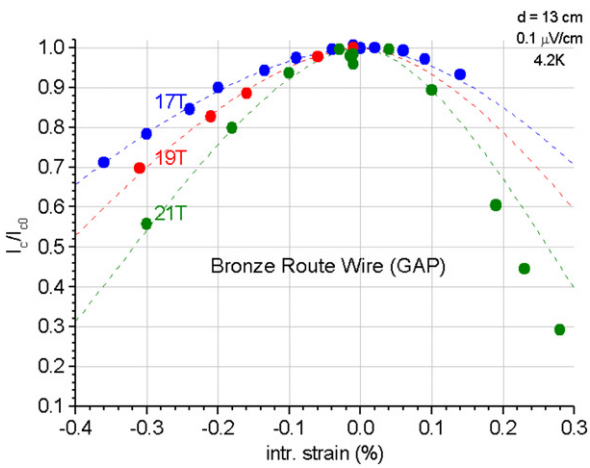

Figure 4. Normalized critical current versus strain at 17, 19 and 21 T at 4.2 K for the bronze route wire (GAP), showing an asymmetric behaviour on both sides of ε_m.

in ΔB_{c2} being of the order of 1 T, while both wires have the same value of $\varepsilon_m = 0.25\%$. Since the estimated difference between binary, i.e. unalloyed, and alloyed Nb_3Sn wires was reported to be 3–4 T in the literature [10–13], it follows that the effect of alloying can be ruled out for explaining the higher strain sensitivity of the internal Sn diffusion wire. This means that the reasons for this difference have to be sought in the individual details of the filament configuration in both wire types, prepared by the bronze route and by internal Sn diffusion.

A first possibility for explaining the stronger sensitivity of $I_c(\varepsilon)/I_{c0}$ for internal Sn diffusion wires could reside in the very different filament sizes of 4 and 80 μm for the bronze route and the internal Sn diffusion wire, respectively (table 1). Indeed, the assumption of an uniaxial (or one-dimensional) model may only be valid for the former, while a full description of internal Sn diffusion wires may require a more complex description,

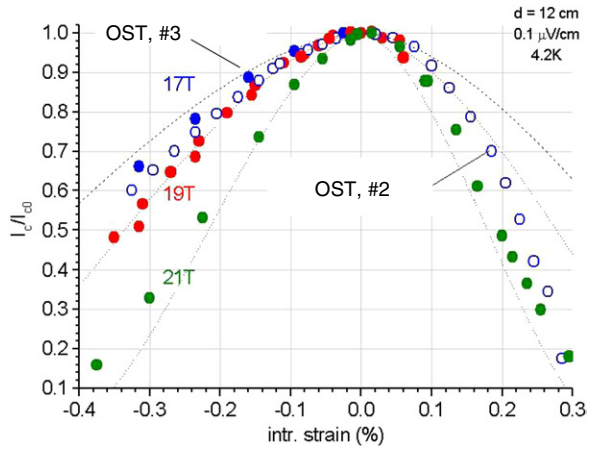

Figure 5. Normalized critical current density versus strain at 17, 19 and 21 T for the internal Sn diffusion wire (OST), showing an asymmetric behaviour on both sides of ε_m. At 17 T, the data of two different pieces of the OST wire are shown.

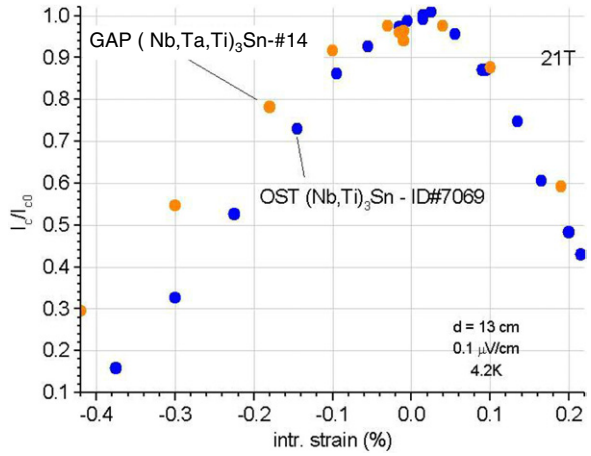

Figure 6. Normalized critical current density versus strain at 21 T for internal Sn diffusion (OST) and bronze route (GAP) wires, showing an asymmetric behaviour on both sides of ε_m.

taking into account 3D stress components. In addition, it is not known whether or not the presence of voids at the centre of the filaments of internal Sn diffusion wires has to be taken into account.

A second explanation is based on the strongly different Sn distribution inside the filaments. Indeed, the Sn composition range in internal Sn wires is comprised between 22 and 25 at.% Sn [15], in contrast to bronze route processed wires, where the composition range is much wider, from 17 to 25 at.% Sn [8, 14]. Like the physical properties of the Nb_3Sn A15 phase, e.g. T_c, B_{c2}, $\rho_0, \ldots$, the mechanical properties are strongly dependent on the Sn content, and the strain behaviour of the Nb_3Sn filaments is thus expected to depend on the distribution of the Sn content in the filaments. In a (Nb, Ta)$_3$Sn bronze route wire, with a Sn content between 18–25 at.%, recent specific heat measurements [16] have confirmed this composition range, revealing that the T_c distribution in the filaments covers the range between 11 and 18 K, with 50% of the filaments being below 17 K. Thus, it is not appropriate

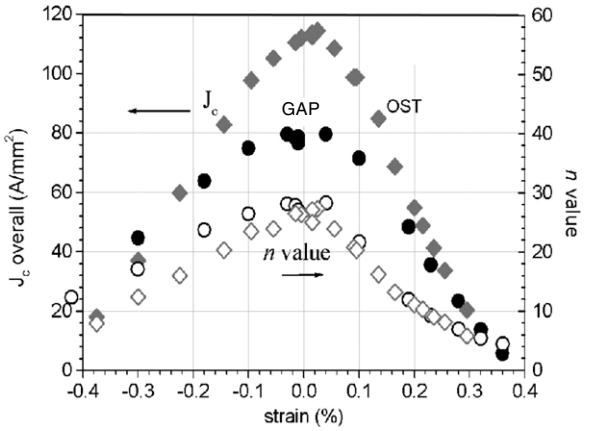

Figure 7. Overall critical current versus uniaxial strain and exponential n value for internal Sn diffusion (OST) and bronze route (GAP) processed Nb_3Sn wires, measured at 21 T and 4.2 K.

to characterize the filaments of Nb_3Sn bronze route wires by average values, neither for the Sn content nor for the value of T_c. This was taken into account by Uglietti *et al* [15], who recently treated the filaments of bronze route wires as composites, with two average compositions, one close to stoichiometry, the other nonstoichiometric (below 22 at.%). This simple model [15] allows one to scale the curves $I_c(\varepsilon)/I_{c0}$ for both wire types, which indicates that the difference between the two wire types can be explained by the different Sn distributions in the filaments.

Empirical descriptions for the behaviour of $J_c(\varepsilon)$ have been given by Ekin [17] and by ten Haken *et al* [18], who defined formulae for fitting $J_c(\varepsilon)$ using different sets of parameters. The main difference between the two models is the dimensionality, Ekin's model [17] being one-dimensional, while ten Haken [18] includes 3D stress components. Taking the appropriate parameters, both models can be used to quantify the slopes of the present $I_c(\varepsilon)/I_{c0}$ curves, shown in figures 5 and 6. The fit for the bronze route (GAP) wires using the model of Ekin [17] showed an excellent agreement, the parameters being $p = 0.5$, $q = 2$, $n = 1$ and $u = 1.7$, i.e. the same ones as in his original paper. This model fits the experimental data at all fields, with a value of the parameter B_{c2} of 25 T at $\varepsilon_{intr} = 0\%$. In order to fit the asymmetric behaviour of $J_c(\varepsilon)$ shown in figures 4–7, the compressive and the tensile state were described by different values for the parameter a [17]. Indeed, for describing the regions ($\varepsilon < \varepsilon_m$) and ($\varepsilon > \varepsilon_m$), the values of a were found to be 900 and 1250, respectively. The only parameter that will be adjusted to fit the data is the critical field at 4.2 K and 0% intrinsic strain, called $B_{c2}(\varepsilon_{intr} = 0\%)$. For the internal Sn diffusion wire the parameter for $\varepsilon < \varepsilon_m$ was found to be $a = 1500$, a value markedly higher than that for bronze route wires.

In ten Haken's model [18], the slope of the $I_c(\varepsilon)$ curve is described by the parameter C_a, which replaces the parameter a in Ekin's formula. When fitting the data for the GAP and the OST wire, one gets C_a values of 33 and 47, respectively. It can thus be seen that both models [17, 18] find a substantial difference between the two parameters a and C_a in both wire types. However, both models furnish only an empirical

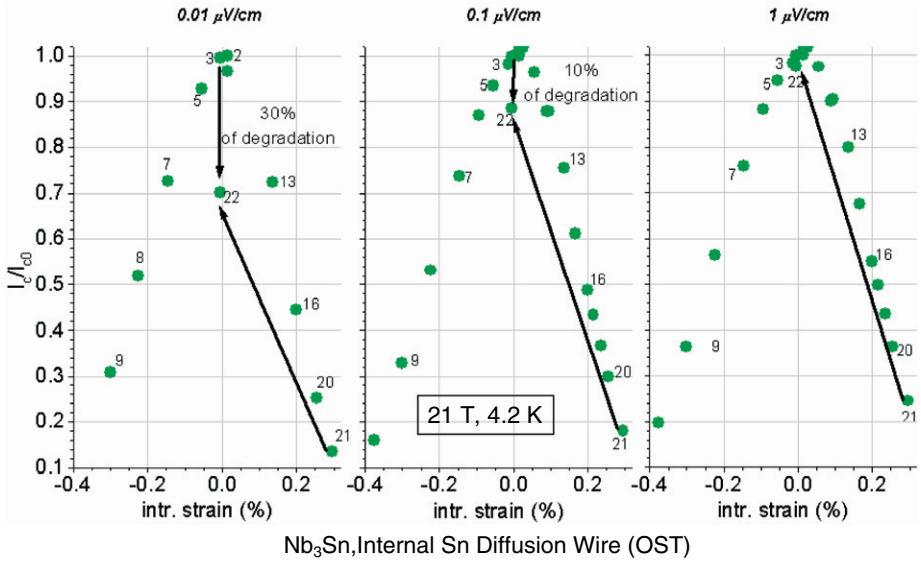

Figure 8. Reduced critical current versus intrinsic strain for the internal Sn diffusion (OST) wire at 21 T, indicating the effect of various voltage criteria. The numbers are labels to identify the sequence of I_c measurements at different strain values. Point #22 is the critical current after recovering from 0.3% intrinsic strain (#21).

description of the phenomenon, and cannot give reasons for the observed difference between the two wire types.

5. The importance of the voltage criterion

At the highest fields, the exponential n values decrease, and J_c depends more and more on the criterion chosen for the determination of J_c, and the possibility to measure much longer wire samples with the WASP constitutes a serious argument in view of a careful characterization.

The advantage of using the WASP can be illustrated on a sample having been strained slightly above ε_{irr}, the irreversible strain value. As an example, the data of $I_c(\varepsilon)/I_{c0}$ for the OST wire are shown in figure 8 after being submitted to an intrinsic strain value of 0.3% (i.e. to a total strain value of 0.55%), which is of course never reached during normal operation. The critical current densities as a function of strain have been determined using the 0.01, 0.1 and 1 μV cm^{-1} criteria, respectively. After applying 0.25% (point #20) of intrinsic strain the $I_c(\varepsilon_{intr} = 0\%)$ (point #2) is fully recovered, even at 0.01 μV cm^{-1}. The situation changes, however, after applying an intrinsic strain of 0.3% (point #21). The $I_c(\varepsilon_{intr} = 0\%)$ is just slightly reduced for 1 μV cm^{-1}, while a reduction of 10% is observed for 0.1 μV cm^{-1}, which even reaches 30% for 0.01 μV cm^{-1} (point #22). The source of degradation may be connected to cracks at a nanometric scale in the filaments. It follows that a sharper voltage criterion for $J_c(\varepsilon)$ is useful for an early detection of filament damage in wires submitted to tensile stresses.

6. The stress distribution inside the filaments and the asymmetry of $J_c(\varepsilon)$

In the following, it will be shown that the observed asymmetry of $I_c(\varepsilon)/I_{c0}$ (figures 4–7) in Nb_3Sn wires is correlated to the tetragonal distortion of the initially cubic A15 lattice. The present consideration is based on earlier diffraction measurements of Flükiger *et al* [19] and Goldacker *et al* [20]. The discussion starts with the stress distribution in bronze route processed Nb_3Sn wires.

6.1. Observation of the stress distribution in Nb_3Sn wires by means of neutron diffraction

The stress distribution inside the filaments of bronze route Nb_3Sn wires (due to the bronze precompression) has been determined by means of neutron diffraction [19]. In contrast to x-ray diffraction, neutron diffraction allows one to determine both tetragonal parameters, a and c, as a function of the angle θ between the wire axis and the neutron beam. The results of the investigation by Goldacker and Flükiger [19, 20], taken on a bundle of bronze route processed wires of the composition Nb–7.5Ta/Cu–13Sn, reacted at 700 °C for 64 h, are reproduced in figure 9. This figure shows the angular dependence of the lattice distortion at the three temperatures: 10, 290 and 473 K. At a fixed temperature, the stress distribution is reflected by the variation of the cell parameters a and c as a function of the filament orientation. It is seen from figure 9 that the cubic A15 phase, characterized by $a = c$, is only present above 500 K, where the Cu–Sn bronze matrix essentially shows a plastic behaviour. With decreasing temperature, the Cu–Sn bronze hardens gradually, thus resulting in an increasing tetragonal distortion of the A15 lattice. At the same time, the lattice undergoes a volume contraction, which will be discussed later (see figure 10). The slight tetragonal distortion, visible at $T = 473$ K, gets more pronounced at 290 K and finally reaches a maximum at 10 K (see figure 9). There $c < a$, the axis c being compressed in the filament direction, while the axis a undergoes an expansion. The measured value of $(1 - c/a)$ at 290 K is 0.0013, and it reaches approximately 0.003 at 10 K. This is considerably lower than the value of $(1 - c/a) = 0.006$ reported for the spontaneously transforming martensitic tetragonal phase in bulk, stress-free Nb_3Sn samples [21].

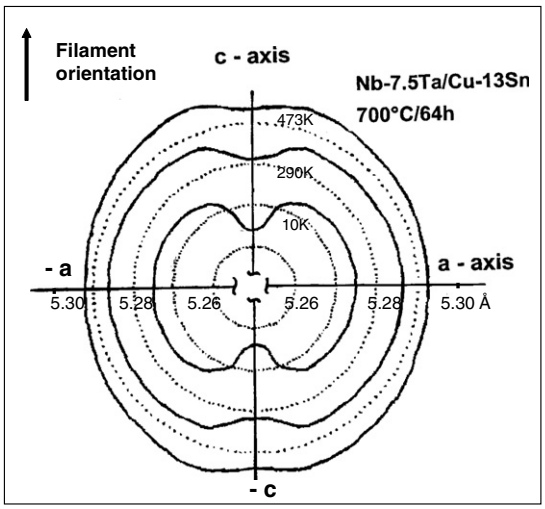

Figure 9. Angular dependence of lattice distortion at 10, 290 and 473 K. The cubic A15 phase at $T > 473$ K undergoes an increasing tetragonal distortion at lower temperatures.

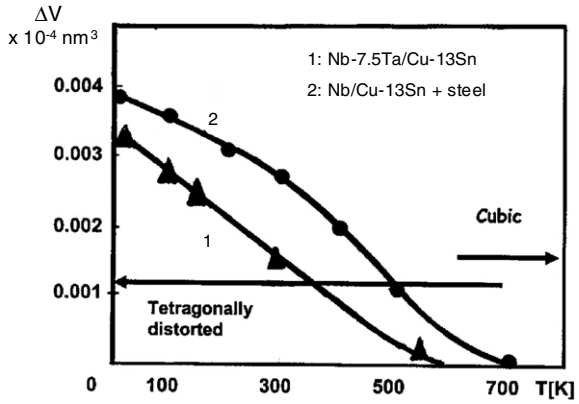

Figure 10. Hydrostatic unit cell volume compression $\Delta V = V_c - V_t$. Figure reprinted and modified from [20]. © 1985 IEEE.

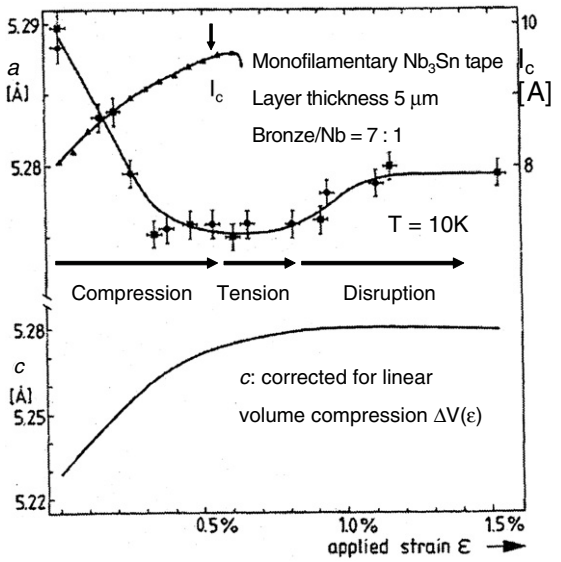

Figure 11. Critical current I_c, lattice parameters a and c versus strain ε. a is measured, while c is calculated after correction for the volume compression $\Delta V(\varepsilon)$: $\Delta V(0) = 0.6\%$ and $\Delta V(1.0\%) = 0$. Figure reprinted and modified from [23]. © 1984 Institut de Physique Fondamentale (IPF).

6.2. The hydrostatic volume compression of Nb_3Sn filaments inside the matrix

As mentioned above, cooling the wires from 500 to 10 K [19, 20] also causes an increasing hydrostatic compression of the unit cell [19, 20]. Indeed, one can compare the volume of the tetragonally distorted unit cell, $V_d(T) = a_d^2(T) \cdot c_d(T)$, and the unstressed cubic cell volume, $V_c(T) = a_c^3(T)$, the latter being obtained by x-ray diffraction measurements on the isolated filaments of the same wire. The experimentally determined hydrostatic volume compression, obtained by subtracting the tetragonal cell from the cubic one, $\Delta V(T) = V_c(T) - V_d(T)$ [19], is shown in figure 10. The hydrostatic pressure can roughly be estimated to 10 kbar, which is too less to cause substantial effects on T_c, B_{c2} and thus on J_c [19].

An example where the hydrostatic compression on the filaments is even stronger has been added to figure 10, showing that the hydrostatic compression $\Delta V(T)$ for an internally steel reinforced Nb_3Sn wire [22] is higher than that without reinforcement. This higher hydrostatic compression is correlated to a higher value of ε_m, which can be as high as 0.8% in steel reinforced wires [22], as a consequence of the higher Young's modulus and the wider elasticity range of steel with respect to Cu–Sn bronze. This example is a further illustration for the direct correlation between elastic deformation and J_c.

6.3. Crystallographic changes in Nb_3Sn wires when applying tensile stress

A direct measurement of the crystallographic changes of the A15 phase inside the filaments when applying tensile stresses at 10 K was first performed by Goldacker and Flükiger [23] by means of x-ray diffraction, on a flat, monofilamentary bronze route Nb_3Sn wire. The bronze/Nb ratio of this sample was 7:1, which explains the relatively high value of $\varepsilon_m = 0.5\%$ (figure 11). For comparison, the bronze/Nb ratio of the bronze wire #24 is lower, 2.5:1. Due to the particular configuration of x-ray diffraction geometry, only the lattice parameters a perpendicular to the wire axis could be measured, which represent the stress-induced radial distortion. It was found that on varying the intrinsic strain $\varepsilon_{intr.}$ of the flat tape from 0 to 0.5%, the lattice parameter a decreased from 5.290 to 5.275 Å (see figure 11). The axial effects (e.g. the lattice parameter c), were calculated by assuming a constant volume of the unit cell at a given temperature, taking into account the volume contraction shown in figure 10. In this work [23], a direct correlation between the variation of the lattice parameters and the critical current density was unambiguously established.

6.4. The asymmetry of $J_c(\varepsilon)$ and the tetragonal distortion

From the above-mentioned diffraction measurements, it is possible to give a reason for the observed asymmetry of $J_c(\varepsilon)$

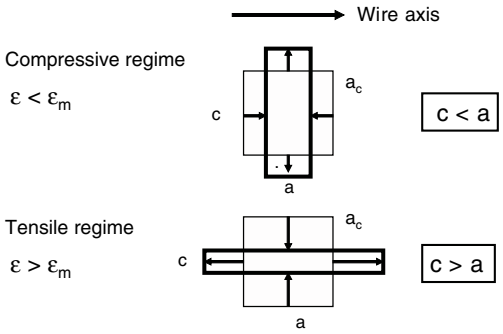

Figure 12. Schematic illustration of the deformation of A15 grains inside a Nb_3Sn filament under precompression by the Cu–Sn bronze, based on the data of [19] and [20]. The tetragonal distortion of the lattice shows an asymmetrical behaviour on both sides of the strain $\varepsilon = \varepsilon_m$.

on both sides of ε_m. At 10 K, without external stresses, the wire is in the compressive regime, and $a > c$, as follows from figure 9. This means that the A15 grains undergo the strongest lattice compression parallel to the wire axis, corresponding to the largest lattice expansion in the radial direction. From [20], it follows that this is the case for all strain values $\varepsilon < \varepsilon_m$. In the tensile regime, where $\varepsilon > \varepsilon_m$, the situation is reversed, and there $c > a$. It is seen from figure 11 that the lattice parameters a and c undergo a different variation under the effect of applied strain. The relative changes of the lattice parameters are shown schematically in figure 12: it is easily seen that the change of a and c cannot be symmetric around ε_m. After having established a direct correlation between the elastic strain and its effects on the critical current density, it follows that an asymmetric change of the 3D strain distribution in the wire involves an asymmetric change of $J_c(\varepsilon)$ on both sides of ε_m. Recently Markiewicz [24] made a further step in the direction of connecting the superconducting critical parameters with the mechanical behaviour via physical equations. The strain dependence of T_c has been calculated starting from the 3D strain state of the A15 layer, by using the strong coupling formalism.

7. Conclusion

The variation of the critical current density, J_c, as a function of the uniaxial applied stress at fields up to 21 T has been measured by means of the modified Walters spring (WASP) on Nb_3Sn wires prepared by both bronze route and internal Sn diffusion processing. The comparison between both wire types shows stronger strain dependence for wires prepared by internal Sn diffusion with respect to those obtained by the bronze route. The reasons for this difference are attributed to the individual details of the filament configuration in both types of wire, for example the homogeneity of the Sn distribution inside the filaments and the filament sizes, of 4 and 80 μm, respectively. More work is necessary to determine the relative importance of both effects on the stronger strain dependence for internal Sn diffusion processed wires.

The results of previous neutron and x-ray diffraction measurements on bronze route processed wires between 10 and 600 K are rediscussed. Neutron diffraction data show that the precompression exerted by the bronze matrix on the filaments causes two effects simultaneously on the A15 filaments.

(1) With decreasing temperature, there is an increasing *hydrostatic volume compression* $\Delta V(T)$, which reaches a maximum of 0.003×10^{-4} nm^{-3} at 10 K. Its influence on J_c is negligible, the change in T_c being very small for a pressure of 10 kbar.

(2) With decreasing temperature, there is a *stress-induced tetragonal deformation*, measurable by the variation of the lattice parameters a and c as a function of temperature, T, and of the angle ϕ between the neutron beam and the wire axis, reflecting the three-dimensional stress distribution in Nb_3Sn filaments. With decreasing temperature, the lattice parameter in the wire direction, c, decreases, while the radial lattice parameter, a, increases. The tetragonality $(1-c/a)$ increases for decreasing T, reaching a maximum of 0.003 at 10 K. The cubic A15 phase is only stable above 500 K, where the bronze matrix is too soft for transmitting shear stresses.

In figure 11 it was shown that the application of uniaxial stress on Nb_3Sn wires leads to a decrease of the tetragonal lattice parameter a, which shows a flat minimum at the strain $\varepsilon = 0$. Combining these results with the observed hydrostatic volume contraction, it follows that the application of tensile strain leads to a shrinking of a and an increase of c, with individual variations being very different on both sides of the strain $\varepsilon = \varepsilon_m$.

From these deformation data, we conclude that the observed asymmetry of $J_c(\varepsilon)$, caused by the non-hydrostatic (or deviatoric) stresses on both sides of the strain ε_m, is connected to an asymmetric change of the 3D stress distribution in the filaments. A confirmation comes from calculations in [24]; explaining the asymmetry of the $J_c(\varepsilon)$ curve goes some way towards an understanding of the fundamental physics behind the $J_c(\varepsilon)$ measurements.

References

[1] Ekin J W, Fickett F R and Clark A F 1977 *Adv. Cryog. Eng.* **22** 449
Ekin J W 1978 *J. Appl. Phys.* **49** 3406
Rupp G 1977 *IEEE Trans. Magn.* **13** 792
[2] ten Haken B, Godeke A and ten Kate H H J 1993 *IEEE Trans. Appl. Supercond.* **3** 1273
Godeke A, Dhallé M, Morelli A, Stobbelaar L, van Weeren H, van Eck H J N, Abbas W, Nijhuis A, den Ouden A and ten Haken B 2004 *Rev. Sci. Instrum.* **75** 5112
[3] Walters C R, Davidson I M and Turck G E 1986 *Cryogenics* **26** 406
[4] Cheggour N and Hampshire D P 2000 *Rev. Sci. Instrum.* **71** 4521
Hampshire D P, Taylor D M, Foley P and Keys S A 2001 *Final Report* No. ITER-Task N11TT119FE
[5] Uglietti D, Seeber B, Abächerli V, Pollini A, Eckert D and Flükiger R 2003 *Supercond. Sci. Technol.* **16** 1000
[6] Uglietti D, Seeber B, Abächerli V, Banno N and Flükiger R 2005 *IEEE Trans. Appl. Supercond.* **15** 3652
[7] Seeber B, Uglietti D, Abächerli V, Bovier P-A, Eckert D, Kübler G, Lezza P, Pollini A and Flükiger R 2005 *Rev. Sci. Instrum.* **76** 1
[8] Abächerli V, Uglietti D, Lezza P, Seeber B, Flükiger R, Cantoni M and Buffat P A 2005 *IEEE Trans. Appl. Supercond.* **15** 3482

[9] Parrell J A, Field M B, Zhang Y and Hong S 2004 *Adv. Cryog. Eng.* **50** 369
[10] Flükiger R, Isernhagen R, Goldacker W and Flükiger R 1983 *Adv. Cryog. Eng.* **30** 851
[11] Specking W, Weiss F and Flükiger R 1987 *IEEE Trans. Magn.* **23** 1188
[12] Sekine H, Togano K and Tachikawa K 1981 *Cryogenics* **21** 152
[13] Takeuchi T, Asano T, Iijima Y and Tachikawa K 1981 *Cryogenics* **21** 585
[14] Klemm M, Seibt E, Specking W and Flükiger R 1990 *Supercond. Sci. Technol.* **3** 249
[15] Uglietti D, Cantoni M, Abächerli V, Seeber B and Flükiger R, 2005 *ICMC (Keystone, USA, Aug. 2005)*; *Adv. Cryog. Eng.* to be published
[16] Wang Y, Senatore C, Abächerli V, Uglietti D and Flükiger R, 2005 *Supercond. Sci. Technol.* **18** submitted
[17] Ekin J 1995 *Cryogenics* **35** S25
[18] ten Haken B, Godeke A and ten Kate H J 1994 *IEEE Trans. Magn.* **30** 1867
[19] Flükiger R, Schauer W, Specking W, Oddi I, Pintschovius L, Müllner W and Lachal B 1982 *Adv. Cryog. Eng.* **28** 361
[20] Goldacker W and Flükiger R 1985 *IEEE Trans. Magn.* **21** 807
[21] Mailfert R, Batterman B W and Hanak J J 1967 *Phys. Lett.* A **24** 315
[22] Flükiger R, Drost E and Specking W 1984 *Adv. Cryog. Eng.* **30** 875
[23] Goldacker W and Flükiger R 1984 *J. Physique* **45** C1 387
[24] Markiewicz W D 2004 *Cryogenics* **44** 895